Dynamical diffraction of neutrons and transition from beam splitter to phase shifter case

Hartmut Lemmel*
Atominstitut der Österreichischen Universitäten, 1020 Wien, Austria
(Received 15 June 2007; revised manuscript received 6 August 2007; published 30 October 2007)

This paper presents formulas for the transmission and the reflection of neutrons on a perfect crystal blade in symmetric Laue geometry. While the standard formulas are valid either for the situation very close to the Bragg condition or far off the Bragg condition (index of refraction model) the formulas presented here smoothly cover the whole range of transition. The paper concludes with experimental considerations.

DOI: 10.1103/PhysRevB.76.144305 PACS number(s): 61.12.−q, 03.75.Dg

I. INTRODUCTION

If neutrons are sent through a beam splitter made of a perfect crystal in Laue geometry [Fig. 1(a)], a very distinct pattern in phase and intensity can be observed, known as the Pendellösung oscillations. The pattern depends on the angle alignment between the beam and the beam splitter on an arcsecond scale. This was demonstrated experimentally by Shull[1,2] and is well understood with the theory of dynamical diffraction.[3–8] On the other hand, if the crystal blade is rotated far off the Bragg condition, it behaves similar to a noncrystalline material [Fig. 1(b)] and can be used as a phase shifter. By rotating the blade up to a few degrees the optical path length is changed due to the index of refraction. This way the phases of interferometry experiments are controlled.

In the recent years more interest has arisen concerning the transition range between the beam splitter case and the phase shifter case. In particular, experiments have been proposed to measure the neutron electron scattering length by precision measurements of the phase and intensity oscillations around the Bragg condition.[9–11] However, the standard solution of the theory of dynamical diffraction does not cover the transition range, as it contains approximations which restrict its validity to the arcsecond scale around the Bragg angle. Depending on the experimental setup and the desired precision, the standard formulas may not be sufficient.

In this paper I derive formulas covering the whole angular range for the symmetrical Laue geometry (Sec. III). Before, I briefly summarize the standard formulas and their limitations (Sec. II). Finally, I discuss experimental considerations concerning the rotation of a Laue crystal through the Bragg condition (Sec. IV).

II. THE STANDARD FORMULAS

A. The beam splitter case

The theory of dynamical diffraction of neutrons is contained in several text books and articles.[4–7] Here I give only a sketch of the derivation of the beam splitter formulas and summarize the results for the transmission factor t and the reflection factor r. The geometry for t and r is illustrated in Fig. 1(a).

The neutron wave function $\psi(\vec{r})$ inside the crystal is calculated by solving the stationary Schrödinger equation on the periodic crystal potential. After transforming the Schrödinger equation into the reciprocal space and using the Bloch ansatz

$$\psi(\vec{r}) = \exp(i\vec{K}\vec{r})\sum_{\vec{H}} u_{\vec{H}} \exp(i\vec{H}\vec{r}) \tag{1}$$

with the sum running over all reciprocal lattice sites, we get an infinite system of coupled equations for the amplitudes $u_{\vec{H}}$

$$\left(\frac{\hbar^2}{2m}|\vec{K}+\vec{H}|^2 - E\right)u_{\vec{H}} = -\sum_{\vec{H}'} V_{\vec{H}'-\vec{H}}u_{\vec{H}'} \tag{2}$$

with the neutron energy E, the neutron mass m, and the Fourier components $V_{\vec{H}}$ of the potential $V(\vec{r})=\Sigma_{\vec{H}}V_{\vec{H}}\exp(i\vec{H}\vec{r})$. In the case of normal Bragg reflection only two reciprocal lattice points lie near the Ewald sphere and the two-beam approximation applies. All but two amplitudes can be set to zero and the infinite system of equations is reduced to two coupled equations for the unknown amplitudes u and u_H which refer to the forward and reflected direction, respectively,

$$\left(\frac{\hbar^2}{2m}K^2 - E\right)u = -V_0 u - V_{-H}u_H, \tag{3a}$$

$$\left(\frac{\hbar^2}{2m}K_H^2 - E\right)u_H = -V_H u - V_0 u_H. \tag{3b}$$

K and K_H denote the absolute values of the forward and the reflected wave vector inside the crystal. The reflected vector is given by $\vec{K}_H=\vec{K}+\vec{H}$ with $\vec{H}$ denoting the reciprocal lattice vector of the reflecting planes.

The potentials V_0 and $V_{\pm H}$ are given by the crystal properties. The general formula is

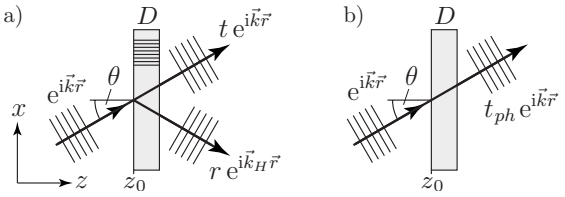

FIG. 1. Sketch of a beam splitter in symmetrical Laue geometry (a) and an ordinary phase shifter (b). The transmission and reflection factors are denoted by t and r (not to be confused with the vector $\vec{r}$).

$$V(\vec{H}) = \frac{2\pi\hbar^2}{mV_c} b_c(\vec{H}) F(\vec{H}), \tag{4}$$

where V_c denotes the volume of the elementary cell, b_c the coherent scattering length, and F the structure factor. For the diamond-type lattice of silicon we can write $V_c = 8/N$ with the atom density N. The structure factor F depends on the Miller indices h,k,l corresponding to $\vec{H}$. For $h+k+l$ divisible by 4 we get $F=8$. For h,k,l all odd we get $F=4\pm 4i$ and for all other cases $F=0$. The scattering length b_c is dominated by the nuclear coherent scattering length b_N. If we take into account the neutron electron scattering length b_{ne} we have to add the term $b_{ne}Z[1-f(\vec{H})]$ with the atomic number Z and the atomic form factor f, see Refs. 9–12. For forward scattering f equals 1 and the b_{ne} term cancels. Collecting all terms we can calculate the forward-scattering potential V_0 and the reflecting potential $V_{\pm H}$ for the commonly used 220 and 111 reflections on silicon:

$$V_0 = \frac{2\pi\hbar^2 N}{m} b_N, \tag{5}$$

$$V_{\pm 220} = \frac{2\pi\hbar^2 N}{m}[b_N + b_{ne} 14(1 - f_{220})], \tag{6}$$

$$V_{\pm 111} = \frac{2\pi\hbar^2 N}{m}[b_N + b_{ne} 14(1 - f_{111})]\frac{1 \pm i}{2}. \tag{7}$$

When solving Eq. (3) one usually makes approximations for small deviations from the Bragg angle and uses the fact that $v_0 = V_0/E$ and $v_H = |V_H|/E$ are in the order of 10^{-6} for thermal neutrons. With the continuity conditions on the crystal surfaces one obtains the standard formulas for the transmission and reflection factors for the symmetric Laue case

$$t = \exp[i(-A_0 - A_H y)]\left\{\cos(A_H\sqrt{1+y^2}) + \frac{iy}{\sqrt{1+y^2}}\sin(A_H\sqrt{1+y^2})\right\}, \tag{8}$$

$$r = \exp[i(-A_0 + A_H y + kz_0 y v_H/\cos\theta_B)]\sqrt{\frac{V_H}{V_{-H}}} \times \frac{-i}{\sqrt{1+y^2}}\sin(A_H\sqrt{1+y^2}). \tag{9}$$

Here we have used the abbreviations

$$A_{0,H} = \frac{\pi D}{\Delta_{0,H}} = \frac{Dkv_{0,H}}{2\cos\theta_B}, \tag{10}$$

$$y = -\delta\theta \sin 2\theta_B / v_H, \tag{11}$$

$$v_0 = V_0/E, \quad v_H = |V_H|/E, \tag{12}$$

where D denotes the blade thickness, $\Delta_0 = \lambda\cos\theta_B/v_0$ the Pendellösung length, λ the neutron wave length, $k = \sqrt{2mE/\hbar^2} = 2\pi/\lambda$ the absolute value of the wave vector, z_0 the position of the crystal blade (Fig. 1), θ_B the Bragg angle for the given wave length and Bragg reflection, θ the incident angle, and $\delta\theta = \theta - \theta_B$ the misset angle, i.e., the deviation from the Bragg angle. The parameter y is a scaled representation of the misset angle.

B. The phase shifter case

The situation of a beam passing a (nonabsorbing) phase shifter, as shown in Fig. 1(b), can be described by the index of refraction $n = \sqrt{1 - V_0/E}$. If we denote the length of the wave vector inside the crystal by $\kappa = nk$ and take into account the continuity of the tangential (x) component we get the transmission factor

$$\begin{aligned} t_{\mathrm{ph}} &= \exp[iD(\kappa_z - k_z)] = \exp[iD(\sqrt{\kappa^2 - k_x^2} - k_z)] \\ &= \exp\{iD[\sqrt{k^2(1 - V_0/E) - k^2\sin^2\theta} - k\cos\theta]\} \\ &= \exp[iDk(\sqrt{\cos^2\theta - v_0} - \cos\theta)]. \end{aligned} \tag{13}$$

As v_0 is in the order of 10^{-6} we can make a first order expansion of the root expression and get

$$t_{\mathrm{ph}} \approx \exp\left(-i\frac{Dkv_0}{2\cos\theta}\right) = \exp\left(-iA_0\frac{\cos\theta_B}{\cos\theta}\right). \tag{14}$$

A further first order expansion for small $\delta\theta \lesssim 1°$ yields

$$t_{\mathrm{ph}} \approx \exp(-iA_0 - iA_0\delta\theta\tan\theta_B). \tag{15}$$

The model of the index of refraction is equivalent to the one-beam approximation of the theory of dynamical diffraction. If the crystal blade is far off the Bragg condition, only the forward amplitude $u_{\vec{0}}$ in Eq. (2) remains, and we would obtain exactly the same result as Eq. (13). Of course, the more amplitudes are included, the more accurate (but also difficult) the calculation will be. This means that the two-beam approximation includes in principle the one-beam approximation. However, this is not achieved by the standard formula (8) due to small angle approximations. If we calculate the asymptotic behavior of Eq. (8) for large misset angles $\delta\theta$ or y we get

$$\lim_{y\to\pm\infty} t = \exp(-iA_0) \tag{16}$$

which is a constant value and clearly cannot serve as a phase shifter formula such as Eq. (15). The standard formula is limited to the arcsecond range around the Bragg angle. In the next section we will rederive formula (8) under the requirement to avoid small angle approximations.

III. THE TWO-BEAM APPROXIMATION FOR LARGE MISSET ANGLES

A. Dispersion surfaces

First we calculate the dispersion surfaces which represent the general solutions of the wave vectors inside the crystal. Looking for a nontrivial solution of equations (3) we get

$$(K^2 - \kappa^2)(K_H^2 - \kappa^2) = k^4\frac{V_{-H}V_H}{E^2} = k^4 v_H^2 \tag{17}$$

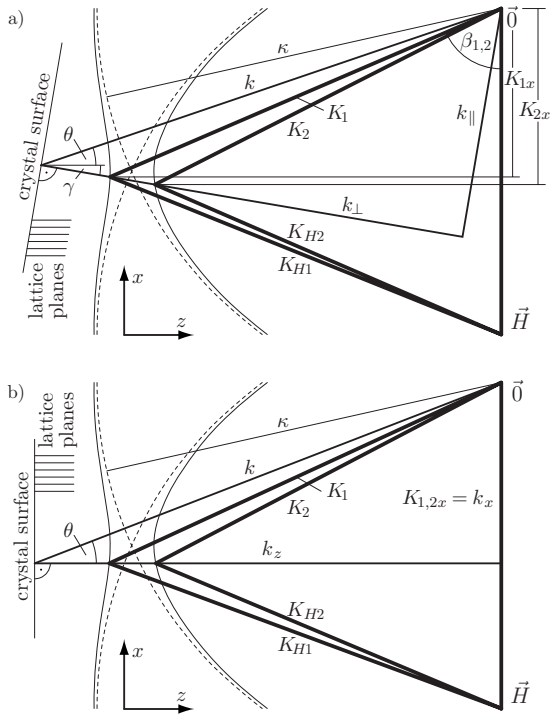

FIG. 2. Sketch of the dispersion surfaces and the construction of the wave vectors inside the crystal for the general (a) and the symmetric (b) Laue case. The dispersion surfaces are given by Eqs. (21) and (22) and approach the circles around $\vec{0}$ and $\vec{H}$ with the radius κ (dashed lines). In the standard approximation for small $\delta\theta$ and $v_{0,H} \approx 10^{-6}$ the dispersion surfaces would be hyperbolas. In this sketch v_0 and v_H have been set to 0.09 in order to give a clear view of the curves. The incident wave vector is given by its absolute value k and the angle θ versus the Bragg planes. In the general case (a) there is an angle γ enclosed between the Bragg planes and the normal of the crystal surface. The incident component $k_\parallel$ parallel to the surface is conserved. Therefore the wave vectors $K_{(H)1,2}$ inside the crystal are given by the intersection points of the dispersion surfaces and the line denoted by $k_\perp$. The situations becomes much simpler in the symmetric case (b) because of $\gamma=0$ and $k_\parallel=k_x=K_{1x}=K_{2x}$.

with $k=\sqrt{2mE/\hbar^2}$ and $\kappa=k\sqrt{1-v_0}$. K and K_H are coupled by

$$\vec{K}_H = \vec{K} + \vec{H}, \tag{18}$$

$$K_H^2 = K^2 + H^2 - 2KH\cos\beta = K^2 + H^2 - 2K_x H \tag{19}$$

with $H=2k\sin\theta_B$, see Fig. 2. Now we take K_x as a given parameter which has to be determined later by the boundary conditions. Then we can insert Eq. (19) into Eq. (17) and get a quadratic equation for K^2

$$(K^2-\kappa^2)(K^2-\kappa^2+H^2-2HK_x) - k^4 v_H^2 = 0 \tag{20}$$

with the two solutions

$$K_{1,2}^2 = \kappa^2 + k^2 v_H(-\eta \pm \sqrt{1+\eta^2}) \tag{21}$$

with

$$\eta := \frac{2\sin\theta_B}{v_H}\left(\sin\theta_B - \frac{K_x}{k}\right). \tag{22}$$

With Eq. (17) we can also calculate K_H:

$$K_{H1,2}^2 = \kappa^2 + k^2 v_H \frac{1}{-\eta \pm \sqrt{1+\eta^2}}. \tag{23}$$

Figure 2 shows the resulting dispersion surfaces. The curves are given by $K_{1,2}$ (or $K_{H1,2}$) as a function of K_x.

B. Boundary conditions

From now on we restrict ourselves to the symmetric Laue case. This is the most common experimental geometry and makes the mathematics a lot easier. It means that the lattice planes are perpendicular to the crystal surface or—in other words—the vector $\vec{H}$ is parallel to the crystal surface, see Fig. 2(b).

1. Front surface

As the tangential component of the wave vector is conserved when entering the crystal, we set $K_x=k_x=k\sin\theta$ and we can write Eq. (22) as

$$\eta = 2\sin\theta_B(\sin\theta_B - \sin\theta)/v_H. \tag{24}$$

If we made a small angle approximation now and set $\sin\theta \approx \sin\theta_B + \delta\theta\cos\theta_B$, we would find that $\eta \equiv y$ and we would get the standard results. But we proceed using the exact expression of η.

In order to calculate the amplitudes $u_{1,2}$ and $u_{H1,2}$ we make the ansatz

$$\psi_{\text{in}} = e^{i\vec{k}\vec{r}}, \tag{25}$$

$$\psi = u_1 e^{i\vec{K}_1\vec{r}} + u_2 e^{i\vec{K}_2\vec{r}} + u_{H1} e^{i\vec{K}_{H1}\vec{r}} + u_{H2} e^{i\vec{K}_{H2}\vec{r}} \tag{26}$$

with

$$\vec{K}_{1,2} = \begin{pmatrix} K_{1,2x} \\ K_{1,2z} \end{pmatrix} = \begin{pmatrix} k_x \\ K_{1,2z} \end{pmatrix}, \tag{27}$$

$$\vec{K}_{H1,2} = \begin{pmatrix} K_{H1,2x} \\ K_{H1,2z} \end{pmatrix} = \begin{pmatrix} k_x - H \\ K_{1,2z} \end{pmatrix}. \tag{28}$$

At the entry surface $z=z_0$ we set $\psi_{\text{in}}=\psi$. Reflections on the surface can be neglected because $E \gg V_0$:

$$e^{ik_z z_0} = u_1 e^{iK_{1z}z_0} + u_2 e^{iK_{2z}z_0} + u_{H1} e^{-iHx} e^{iK_{1z}z_0} + u_{H2} e^{-iHx} e^{iK_{2z}z_0}. \tag{29}$$

As this equation must hold for all x it splits into two parts

$$u_1 e^{iK_{1z}z_0} + u_2 e^{iK_{2z}z_0} = e^{ik_z z_0}, \tag{30}$$

$$u_{H1} e^{iK_{1z}z_0} + u_{H2} e^{iK_{2z}z_0} = 0. \tag{31}$$

From Eqs. (3a) and (21) we get the relation

$$u_{H1,2} = u_{1,2}\frac{\kappa^2 - K_{1,2}^2}{k^2 V_{-H}/E} = u_{1,2}(\eta \mp \sqrt{1+\eta^2})\sqrt{\frac{V_H}{V_{-H}}}. \quad (32)$$

Here we have used the fact that $|V_H|/V_{-H} = \sqrt{V_H/V_{-H}}$ because of $V_{-H} = V_H^*$. From the last three equations we finally get the amplitudes inside the crystal:

$$u_1 = \exp[i(k_z - K_{1z})z_0]\frac{\sqrt{1+\eta^2}+\eta}{2\sqrt{1+\eta^2}}, \quad (33)$$

$$u_2 = \exp[i(k_z - K_{2z})z_0]\frac{\sqrt{1+\eta^2}-\eta}{2\sqrt{1+\eta^2}}, \quad (34)$$

$$u_{H1} = \exp[i(k_z - K_{1z})z_0]\frac{-1}{2\sqrt{1+\eta^2}}\sqrt{\frac{V_H}{V_{-H}}}, \quad (35)$$

$$u_{H2} = \exp[i(k_z - K_{2z})z_0]\frac{1}{2\sqrt{1+\eta^2}}\sqrt{\frac{V_H}{V_{-H}}}. \quad (36)$$

2. Back surface

The back surface is assumed to be parallel to the front surface, enclosing a crystal of the thickness D. The transmitted wave vector is equal to the incident wave vector because of the conserved x component k_x and the conserved energy. The reflected wave vector $\vec{k}_H$ is determined by the Bragg reflection $k_{Hx} = k_x - H$ and by the energy conservation $k_{Hz} = \sqrt{k^2 - k_{Hx}^2}$. With these wave vectors we can make the following ansatz for the transmission factor t and the reflection factor r (as illustrated in Fig. 1):

$$\psi_O = te^{i\vec{k}\vec{r}}, \quad (37)$$

$$\psi_H = re^{i\vec{k}_H\vec{r}}. \quad (38)$$

On the back surface $z = D + z_0$ the inner wave function ψ Eq. (26) and the outer wave function $\psi_O + \psi_H$ must be equal. The resulting equation splits again into two parts in order to be fulfilled for all x and we get

$$t = e^{-ik_z D}\left(\frac{e^{iK_{1z}D} + e^{iK_{2z}D}}{2} + \frac{\eta}{\sqrt{1+\eta^2}}\frac{e^{iK_{1z}D} - e^{iK_{2z}D}}{2}\right), \quad (39)$$

$$r = e^{-ik_z D}e^{i(k_z - k_{Hz})(D+z_0)}\sqrt{\frac{V_H}{V_{-H}}}\frac{-1}{\sqrt{1+\eta^2}}\frac{e^{iK_{1z}D} - e^{iK_{2z}D}}{2}. \quad (40)$$

Now we need the terms $K_{1,2z}$, k_{Hz}, and k_z which depend on the incident angle θ. So does η (24). Because we want to stick to the exact expression of η, we use η as input parameter and express instead $K_{1,2z}$, k_{Hz} and k_z in terms of η. Inverting Eq. (24) we get

$$\sin\theta = \sin\theta_B - v_H\frac{\eta}{2\sin\theta_B}, \quad (41)$$

$$K_{1,2z} = \sqrt{K_{1,2}^2 - K_{1,2x}^2} = \sqrt{K_{1,2}^2 - k^2\sin^2\theta} = k\sqrt{\cos^2\theta_B - v_0 \pm v_H\sqrt{1+\eta^2} - v_H^2\eta^2\frac{1}{4\sin^2\theta_B}}, \quad (42)$$

$$k_{Hz} = \sqrt{k^2 - (k_x - H)^2} = k\sqrt{1 - (\sin\theta - 2\sin\theta_B)^2} = k\sqrt{\cos^2\theta_B - v_H\eta - v_H^2\eta^2\frac{1}{4\sin^2\theta_B}}, \quad (43)$$

$$k_z = k\cos\theta = k\sqrt{1-\sin^2\theta} = k\sqrt{\cos^2\theta_B + v_H\eta - v_H^2\eta^2\frac{1}{4\sin^2\theta_B}}. \quad (44)$$

Up to this point no approximation has been used. Now we expand the root expressions (42)–(44) in terms of v_0 and v_H which are, as stated before, in the order of 10^{-6}. The results below are already given as the difference terms $DK_{1,2z} - Dk_z$ and $(k_z - k_{Hz})(D + z_0)$ because these terms have to be inserted into t (39) and r (40).

First order expansion:

$$DK_{1,2z} - Dk_z = -A_0 - A_H\eta \pm A_H\sqrt{1+\eta^2}, \quad (45)$$

$$(k_z - k_{Hz})(D + z_0) = 2A_H\eta + z_0\eta k v_H/\cos\theta_B. \quad (46)$$

With these expressions, t and r yield exactly the standard results (8) and (9) if we finally make a small angle approximation and replace η by y.

Second order expansion:

$$DK_{1,2zz} - Dk_z = -A_0(1+\bar{\varepsilon}) - A_H\eta \pm A_H\sqrt{1+\eta^2}(1+\varepsilon) \quad (47)$$

with

$$\bar{\varepsilon} = \varepsilon\frac{1 + v_H^2/v_0^2}{2}, \quad \varepsilon = \frac{v_0}{2\cos^2\theta_B}. \quad (48)$$

Expression (46) remains the same also in second order. Inserting these expressions in Eqs. (39) and (40) we get

$$t = \exp[-iA_0(1+\bar{\varepsilon}) - iA_H\eta]\left\{\cos[A_H\sqrt{1+\eta^2}(1+\varepsilon)] + \frac{i\eta}{\sqrt{1+\eta^2}}\sin[A_H\sqrt{1+\eta^2}(1+\varepsilon)]\right\}, \quad (49)$$

$$r = \exp[-iA_0(1+\bar{\varepsilon}) + iA_H\eta + iz_0\eta k v_H/\cos\theta_B]\sqrt{\frac{V_H}{V_{-H}}} \times \frac{-i}{\sqrt{1+\eta^2}}\sin[A_H\sqrt{1+\eta^2}(1+\varepsilon)]. \quad (50)$$

These results look very similar to the standard results except for the little parameters ε and $\bar{\varepsilon}$. Both are in the order of 10^{-6} and are added to unity. So why does it make so much difference? The answer is, that the term $(1+\varepsilon)$ is part of a phase term which always counts modulo 2π. Although the relative

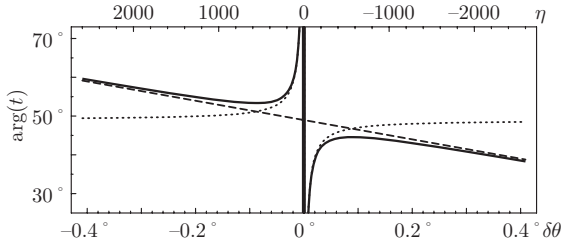

FIG. 3. The argument value of the new transmission formula (49) is plotted by the solid line. The dotted line shows the standard transmission formula (8) and the dashed line shows the phase shifter formula (15). The curves have been calculated for $D=1$ mm and $\theta_B=30°$, using a silicon (220) reflection. For these parameters and $\delta\theta=0$, the phase shift given by Eq. (15) amounts to $-A_0=-43.13$. This value modulo 2π is roughly 49° which can be recognized in the plot. The thick vertical line at $\delta\theta=0$ actually represents a phase change over many orders of 2π as shown in Fig. 4.

phase change is in the ppm range, it can be blown up to a considerable change of the absolute phase if it is multiplied by a large factor. $\sqrt{1+\eta^2}$ does become large if we get far away from the Bragg condition. Only $\bar{\varepsilon}$ can be dropped because A_0 is in the order of 10^2 and $A_0\bar{\varepsilon}\approx 10^{-4}\ll 2\pi$.

For comparison with the phase shifter formula we calculate the limit of t for large η:

$$\lim_{\eta\to\pm\infty}\sqrt{1+\eta^2}=|\eta|, \tag{51}$$

$$\begin{aligned}\lim_{\eta\to\pm\infty} t &= \exp(-iA_0-iA_H\eta)\left\{\cos[A_H|\eta|(1+\varepsilon)]\right.\\ &\left.+\frac{i\eta}{|\eta|}\sin[A_H|\eta|(1+\varepsilon)]\right\}\\ &=\exp(-iA_0-iA_H\eta)\exp[iA_H\eta(1+\varepsilon)]\\ &=\exp(-iA_0+iA_H\eta\varepsilon)\\ &=\exp[-iA_0+iA_0\tan\theta_B(\sin\theta_B-\sin\theta)/\cos\theta_B]\\ &\approx\exp(-iA_0-iA_0\,\delta\theta\tan\theta_B),\quad |\delta\theta|\lesssim 1°. \end{aligned}\tag{52}$$

Now we have obtained the phase shifter result (15), proving that formula (49) smoothly covers the whole range from the beam splitter to the phase shifter case. Figure 3 shows the differences between the formulas.

The neutron electron scattering length is contained in A_H and in η. However, it cancels in the product $A_H\eta$ because v_H cancels:

$$A_H\eta=\frac{Dkv_H}{2\cos\theta_B}\,\frac{2\sin\theta_B(\sin\theta_B-\sin\theta)}{v_H}.$$

This means that the neutron electron scattering length only enters in the braced term of (49) and only for η small enough so that $\sqrt{1+\eta^2}\neq\eta$. (As stated before, the term $\bar{\varepsilon}$ can be neglected.)

3. Approximations for small $\delta\theta$

Finally we can make a first order approximation of $\sin(\theta_B+\delta\theta)$ for small $\delta\theta$ if we are only interested in the near range around the Bragg condition, $|\delta\theta|\lesssim 1°$. This range includes not only the Bragg reflection itself but also the transition range to the phase shifter regime, see Fig. 3.

$$\eta=\frac{2\sin\theta_B[\sin\theta_B-\sin(\theta_B+\delta\theta)]}{v_H}\approx-\frac{\delta\theta\sin 2\theta_B}{v_H}=y. \tag{53}$$

The resulting formulas of the transmission and reflection factors are

$$\begin{aligned}t=\exp(-iA_0-iA_Hy)&\left\{\cos[A_H\sqrt{1+y^2}(1+\varepsilon)]\right.\\ &\left.+\frac{iy}{\sqrt{1+y^2}}\sin[A_H\sqrt{1+y^2}(1+\varepsilon)]\right\},\end{aligned}\tag{54}$$

$$\begin{aligned}r=\exp(-iA_0+iA_Hy+iz_0ykv_H/\cos\theta_B)&\sqrt{\frac{V_H}{V_{-H}}}\\ &\times\frac{-i}{\sqrt{1+y^2}}\sin[A_H\sqrt{1+y^2}(1+\varepsilon)].\end{aligned}\tag{55}$$

In Fig. 3, Eq. (54) could not be distinguished from Eq. (49).

IV. DISCUSSION

A. Interpretation of the transmitted phase

If we plot the transmission factor more closely around the Bragg condition (Fig. 4) we notice that the argument value of

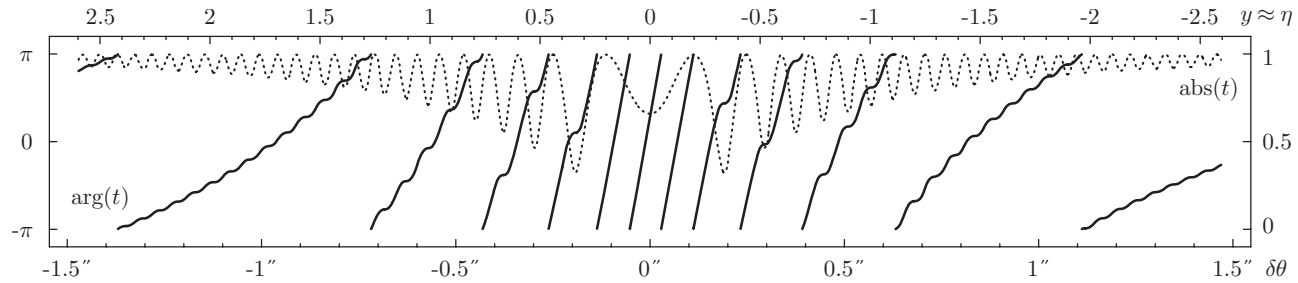

FIG. 4. Plot of the transmission factor t closely around the Bragg condition. In this regime there is virtually no difference between the standard Eq. (8) and the new formula (49). The absolute value of t (dotted line) scales on the right side. The argument value (solid line) scales on the left side. The parameters are $D=1$ mm and $\lambda=2$ Å on a silicon 220 crystal ($A_0=A_H=43.13$).

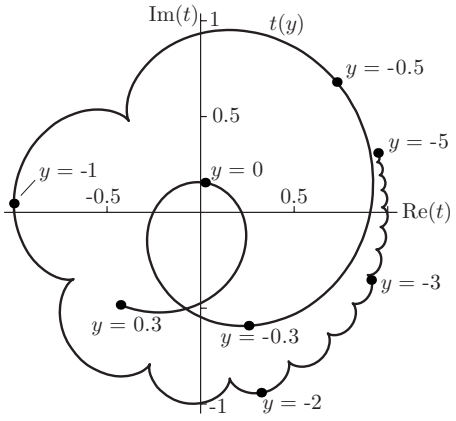

FIG. 5. A parametric plot of $t(y)$ in the complex plane. Far away from the Bragg condition the curve approaches a circle with radius one because the transmitted amplitude $|t|$ is one. Coming close to the Bragg condition the curve rotates around the origin and develops curly features. In order to give a clear view the parameters A_0 and A_H have been set to the arbitrary value of 3.55π. This would correspond to a crystal thickness in the order of 0.25 mm.

t grows faster and faster as we come close to the Bragg condition. It seems to be a monotonic increasing function (solid line in Fig. 4) although it approaches the same asymptote (dashed straight line in Fig. 3) for large positive and negative values of $\delta\theta$. A paradox? It depends on the way of plotting. The argument function gives the phase modulo 2π which results in the "phase jumps" shown in Fig. 4. We could also plot the phase as a continuous function but in this case we would obtain two different asymptotes. However, these asymptotes would be separated exactly by a multiple of 2π and would therefore be physically identical.

For a better understanding, a parametric plot of $t(y)$ in the complex plane is given in Fig. 5. t rotates around the origin as a function of y. The curve contains curly features which develop into loops if the crystal thickness is increased (parameters $A_{0,H}$). If one of the loops comes close to the origin [see Fig. 6(a)] then the argument function of t approaches a π step. If the crystal thickness is further increased and the curve crosses the origin, then the π step is inverted [see Fig. 6(b)]. This way the distance of the asymptotes is changed by exactly 2π each time another loop crosses the origin.

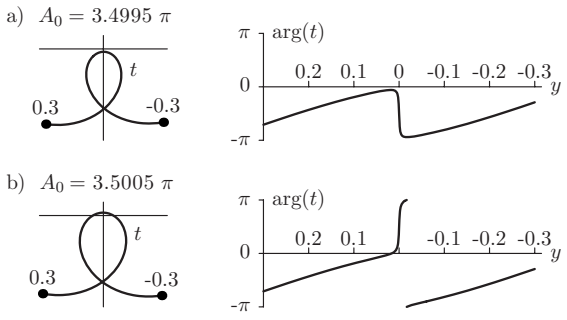

FIG. 6. If the crystal thickness (parameter A_0) is increased, more and more of the curls shown in Fig. 5 cross the origin. Each crossing changes a negative π step of the argument function (a) into a positive π step (b), inserting exactly 2π between the asymptotes for large positive and negatie values of y.

B. Experimental requirements

The phase of the transmission factor can be measured by putting the Laue crystal into an interferometer and rotating it carefully through the Bragg condition. Such an experiment has been performed by Graeff in 1978.[13] Related experiments have been performed with the sample crystal in Bragg geometry[14] and again in Laue geometry but with x rays.[15] New experiments have been proposed during the last years, motivated by the prospect of measuring the neutron electron scattering length.[10,11]

The experiment by Graeff covered the transition range $0.0015° < |\delta\theta| < 0.015°$ and showed that the slope of $\arg(t)$ became steeper and steeper as the Bragg condition was approached. Unfortunately no quantitative analysis of the measured phase values was published. The effect of the new transmission formula should have been observable. Furthermore, the range closer to the Bragg condition $|\delta\theta| < 0.0015°$ could not be accessed at all. The reason is, that the visibility of the interference fringes is limited by two factors, which become quite severe close to the Bragg condition.

First, the measured phase is always averaged over the beam divergence. If the argument value of t changes by more than 2π within the beam divergence then the visibility of the interference fringes will vanish. This means that the beam divergence should be less than $y \approx 0.1$ or $\delta\theta \approx 2 \times 10^{-5°} \approx 0.07$ arcseconds if we want to resolve the steep slope of $\arg(t)$ in the center of Fig. 4. This could be achieved by placing a narrow slit mask of a neutron absorber onto the front and the back surface of the first interferometer crystal.[16] Of course, the drawback would be a strongly reduced beam intensity, making precision measurements very difficult.

Second, we have to consider defocusing effects which are caused by the sweep of the probability current density within the Borrmann triangle,[6,17] especially if we use a highly collimated beam and thick sample blades. In order to describe this effect we have to deal with localized beams instead of plain waves. Localized beams are described by spherical theories which can be found in Refs. 4–8. Here we use a numerical superposition of the plain wave formulas. The details of this approach are given in the appendix. Figure 7 shows the Laue transmission of a localized beam for different misset angles. We can see that the transmitted beam is split and transversally displaced as we approach the Bragg condition. At $y=0$ the beam is shifted sidewards by $D \sin \theta_B$. If such a sample is inserted into an interferometer, the interferometer will be defocused, and the visibility of the interference pattern will be reduced if not destroyed. In addition, the results of the phase measurement would be questionable because the level of defocusing changes during the measurement, when the crystal is rotated. The problem could be reduced with small values of D and θ_B but not completely solved. Here I want to propose a compensating setup which keeps the interferometer focused (Fig. 8).

In each beam path there is a sample crystal before and after the mirror blade. The sample crystals can be rotated

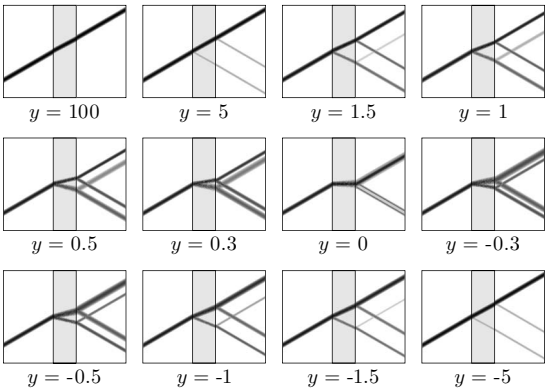

FIG. 7. The wave function of a localized beam passing a crystal under different misset parameters y. The crystal (gray rectangle) is 3 mm thick. The intensity of the wave function is shown in gray shades and has been calculated for a beam divergence of σ_y=0.1 and a beam width of σ_w=0.1 mm.

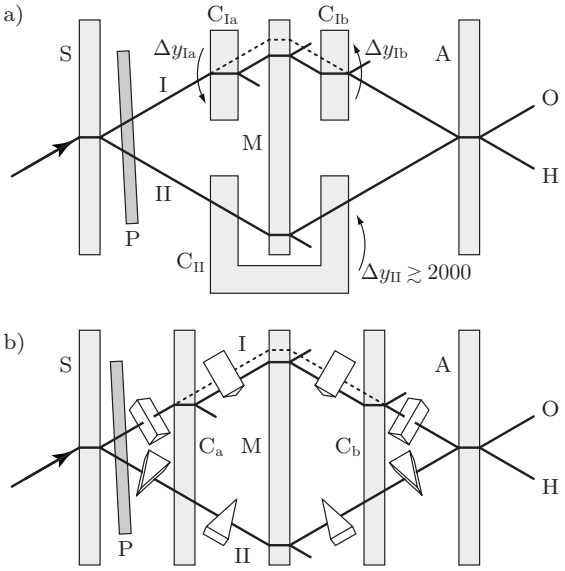

FIG. 8. Setups for measuring the phase shift from Laue transmission without defocusing the interferometer. (a) A standard perfect crystal interferometer is given by the three blades S (splitter), M (mirror), and A (analyzer). The crystals C_{Ia} and C_{Ib} are to be measured and intersect beam I before and after the mirror. This compensates the transverse beam displacement within the Borrmann triangle and keeps the interferometer focused as long as the rotation parameters Δy_{Ia} and Δy_{Ib} have the same absolute value. However, the precision alignment of the crystals C_{Ia} and C_{Ib} is very challenging (Ref. 10). (b) The equivalent setup using a five blade interferometer and prisms. The blades C_a and C_b serve as samples and are fixed monolithically to the interferometer in order to avoid the crystal alignment. Instead of rotating the crystals, the beam direction is changed by the use of prisms (Refs. 11, 18, and 19). The degree of beam deflection within the interferometer plane is controlled by rotating the prisms around the beam axis. However, this setup is very challenging either because of the large number of prisms to align and because the interferometer has to be very large to give enough space for the prisms.

[Fig. 8(a)] or, alternatively, the beams around the samples can be deflected by the use of prisms [Fig. 8(b)]. For the sake of simplicity we stick to the sample rotation picture for the further argumentation.

If both samples within one beam path are rotated by the same misset angle then the transverse displacement of the beam by one crystal is reversed by the other and the interferometer is kept focused. This can be achieved by a monolithic design of both sample crystals such as crystal C_{II} in Fig. 8(a). Alternatively we could rotate the crystals by the same amount but in opposite directions. The interferometer would still be focused, as we can see from Fig. 7 where the beam trajectories through the samples are quite similar for y and $-y$.

Now we calculate the resulting phases for both cases. We look at a single plane wave component with the misset parameter y_0 with respect to the interferometer crystals. We denote the rotation of the two sample crystals in beam I by Δy_{Ia} and Δy_{Ib}. Then the first crystal C_{Ia} contributes $t(y_0+\Delta y_{\mathrm{Ia}})$ to the wave function, with $t(y)$ given by Eq. (54). The second crystal C_{Ib} contributes $t(-y_0-\Delta y_{\mathrm{Ib}})$ because the orientation of the y scale is reversed by the reflection on the mirror blade.

If $\Delta y_{\mathrm{Ia}}=\Delta y_{\mathrm{Ib}}$ then the total sample contribution in beam I is given by

$$t(y)t(-y) = \exp(-i2A_0)\left\{\cos^2[A_H\sqrt{1+y^2}(1+\varepsilon)] + \frac{y^2}{1+y^2}\sin^2[A_H\sqrt{1+y^2}(1+\varepsilon)]\right\} \quad (56)$$

with $y=y_0+\Delta y_{\mathrm{Ia}}$. We can see that the argument value of this expression amounts to the constant value $-2A_0$. It does not depend on y which means that all plane wave components yield the same phase shift. Nor does it depend on A_H which means that it is completely insensitive to the neutron electron scattering length. We can use this sample configuration for the compensating crystal C_{II} in the reference beam. We do not even have to care much about the alignment of this crystal. If we rotate it far off the Bragg condition the braced expression in Eq. (56) becomes 1.

If $\Delta y_{\mathrm{Ia}}=-\Delta y_{\mathrm{Ib}}$ then we get the rather complicated expression $t(y_0+\Delta y_{\mathrm{Ia}})t(-y_0+\Delta y_{\mathrm{Ia}})$. For $y_0=0$ it simplifies to $t(\Delta y_{\mathrm{Ia}})^2$. This is finally the sample configuration we can use to measure the phase of the Laue transmission factor without defocusing the interferometer. However, we have to align two sample crystals precisely to the interferometer crystal and rotate them in opposite directions. It still has to be shown whether this—or the alternative setup with prisms—is experimentally feasible.

C. Conclusion and outlook

We have derived a mathematical description of the symmetric Laue case, which is not restricted to small deviations from the Bragg condition but covers the whole angular range from the beam splitter case to the phase shifter case. The theory establishes a more profound basis for experiments which make use of the phase shift around the Bragg condi-

tion, such as measuring the neutron electron scattering length in a neutron interferometer.[10,11,18]

Basic ideas about experimental setups for measuring the phase of the Laue transmission factor have been presented. However there is still need to estimate the magnitude of the measured quantities under real experimental conditions, and to determine the accuracy to which the neutron electron scattering length could be obtained. An interferometer simulation program is under developement for calculating the neutron wave function at any point of interferometer setups as shown in Fig. 8.

ACKNOWLEDGMENT

This work was supported by the projects P18460-N16 and F15-P13 of the Austrian Science Fund (FWF).

APPENDIX: CREATING LOCALIZED BEAMS FROM PLANE WAVES

We have derived plane wave formulas such as Eq. (54) and want to calculate the wave function of a localized beam which is characterized by its width and divergence. As before we calculate in two dimensions x and z.

With a given angular distribution $g_\theta(\theta)$ and the fact that we are dealing with time independent monoenergetic solutions of the Schrödinger equation, we can write the wave function in k space in polar coordinates as $\psi(k,\theta)=\delta(k-k_0)g_\theta(\theta)$. The Fourier transform gives the wave function in real space.

$$\psi(\vec{r}) = \frac{1}{2\pi}\int d^2k e^{i\vec{k}\cdot\vec{r}}\psi(\vec{k}) = \frac{1}{2\pi}\int_{-\pi}^{\pi} d\theta \int_0^\infty k dk e^{i\vec{k}\cdot\vec{r}}\psi(k,\theta)$$

$$= \frac{k_0}{2\pi}\int_{-\pi}^{\pi} d\theta e^{i\vec{k}_0\cdot\vec{r}} g_\theta(\theta). \tag{A1}$$

This wave function corresponds to a point source at the origin, shining in the directions given by g_θ. For the further calculation we drop the index in k_0.

Now we calculate the beam width for a given distance from the source. We assume $g_\theta(\theta)$ to be a narrow Gaussian distribution $\exp[-(\theta-\theta_B)^2/(2\sigma_\theta^2)]/\sqrt{2\pi\sigma_\theta^2}$. Then it can be shown that the transverse intensity profile is again a Gaussian distribution if we go far away from the source. Using l as longitudinal beam coordinate and w as transverse coordinate we can write

$$|\psi(l,w)|^2 = \frac{1}{\sqrt{1+k^2l^2\sigma_\theta^4}}\exp\left(-\frac{w^2}{2\sigma_w^2}\right), \tag{A2}$$

$$\sigma_w = \sqrt{\frac{1}{2}\left(\frac{1}{k^2\sigma_\theta^2}+\sigma_\theta^2 l^2\right)}. \tag{A3}$$

Formula (A3) tells us the beam width σ_w at the distance l from the source for a given beam divergence σ_θ. This way we can calculate the position $\vec{r}_0$ of the source if we want the beam to have a certain width at the crystal position.

With Eq. (53) we switch from $\delta\theta$ and σ_θ to y and σ_y. Then the incident, transmitted and reflected wave functions are given by

$$\psi_{\text{in}}(\vec{r}) = \int dy g(y)\exp[i\vec{k}(y)\cdot(\vec{r}-\vec{r}_0)], \tag{A4}$$

$$\psi_t(\vec{r}) = \int dy g(y)t(y)\exp[i\vec{k}(y)\cdot(\vec{r}-\vec{r}_0)], \tag{A5}$$

$$\psi_r(\vec{r}) = \int dy g(y)r(y)\exp[i\vec{k}_H(y)\cdot(\vec{r}-\vec{r}_0)], \tag{A6}$$

$$g(y) = \frac{1}{\sqrt{2\pi}\sigma_y}\exp\left(-\frac{y^2}{2\sigma_y^2}\right). \tag{A7}$$

The integrals have to be solved numerically for each point $\vec{r}$. If the integral is replaced by a sum with step size Δy we get artificial duplicates of the beam with a transverse offset of $w=\lambda/\Delta\theta$ where $\Delta\theta$ denotes the step size Δy in radiant units according to Eq. (53). We have to choose the step size $\Delta\theta$ small enough so that the artifacts lie outside the region of interest $\Delta\theta \lesssim \lambda/w$. For a neutron wavelength of $\lambda=2$ Å and a beam width w of a few mm we get $\Delta\theta \lesssim 10^{-8}$ or $\Delta y \lesssim 0.01$. In addition we have to ensure that Δy is small enough to resolve the Pendellösung fringes, see dotted line in Fig. 4.

This approach can be easily extended to a whole interferometer or any other arrangement of crystal blades. A computer program for general neutron interferometer simulations is under development by the author.

*hartmut@lemmel.at

[1] C. G. Shull, Phys. Rev. Lett. **21**, 1585 (1968).
[2] C. G. Shull and J. A. Oberteuffer, Phys. Rev. Lett. **29**, 871 (1972).
[3] B. W. Batterman and H. Cole, Rev. Mod. Phys. **36**, 681 (1964).
[4] H. Rauch and D. Petrascheck, *Dynamical Neutron Diffraction and Its Application* (Springer-Verlag, Berlin, 1978), Chap. 9.
[5] S. A. Werner, Phys. Rev. B **21**, 1774 (1980).
[6] H. Rauch and S. A. Werner, *Neutron Interferometry* (Clarendon Press, Oxford, 2000).
[7] D. Petrascheck and R. Folk, Phys. Status Solidi A **36**, 147 (1976).
[8] U. Bonse and W. Graeff, *X-Ray Optics*, Vol. 22 of *Topics in Applied Physics* (Springer Verlag, Heidelberg, 1977), Chap. X-Ray and Neutron Interferometry.
[9] J.-M. Sparenberg and H. Leeb, J. Electron Spectrosc. Relat. Phenom. **129**, 315 (2003).
[10] F. E. Wietfeldt, M. Huber, T. C. Black, H. Kaiser, M. Arif, D. L. Jacobson, and S. A. Werner, Physica B **385-386**, 1374 (2005).
[11] A. Ioffe and M. Vrana, Appl. Phys. A **74**, S314 (2002).
[12] V. F. Sears, Phys. Rep. **141**, 281 (1986).

[13] W. Graeff, W. Bauspiess, U. Bonse, and H. Rauch, Acta Crystallogr., Sect. A: Cryst. Phys., Diffr., Theor. Gen. Crystallogr. **34**, S238 (1978).
[14] H. Rauch, Nucl. Instrum. Methods Phys. Res. A **284**, 156 (1989).
[15] K. Hirano and A. Momose, Phys. Rev. Lett. **76**, 3735 (1996).
[16] S. Kikuta, I. Ishikawa, K. Kohra, and S. Hoshino, J. Phys. Soc. Jpn. **39**, 471 (1975).
[17] G. Borrmann, Naturwiss. **42**, 67 (1955).
[18] The interferometer group at the Atominstitut has initiated a project (P18460-N16) for measuring phase effects due to dynamical diffraction and coherence properties of large scale interferometers by means of prism refraction.
[19] U. Bonse, W. Graeff, and H. Rauch, Phys. Lett. **69A**, 420 (1979).